

nnUNet_RASPP for Retinal OCT Fluid Detection, Segmentation and Generalisation over Variations of Data Sources

Nchongmaje Ndipenoch, Alina Miron, Zidong Wang and Yongmin Li

Department of Computer Science, Brunel University London, Uxbridge, UB8 3PH, United Kingdom

Abstract. Retinal Optical Coherence Tomography (OCT), a noninvasive cross-sectional scan of the eye with qualitative 3D visualization of the retinal anatomy is used to study the retinal structure and the presence of pathogens. The advent of the retinal OCT has transformed ophthalmology and it is currently paramount for the diagnosis, monitoring and treatment of many eye pathogens including Macular Edema which impairs vision severely or Glaucoma that can cause irreversible blindness. However the quality of retinal OCT images varies among device manufacturers. Deep Learning methods have had their success in the medical image segmentation community but it is still not clear if the level of success can be generalised across OCT images collected from different device vendors. In this work we propose two variants of the nnUNet [8]. The standard nnUNet and an enhanced version called nnUNet_RASPP (nnU-Net with residual and Atrous Spatial Pyramid Pooling) both of which are robust and generalise with consistent high performance across images from multiple device vendors. The algorithm was validated on the MICCAI 2017 RETOUCH challenge dataset [1] acquired from 3 device vendors across 3 medical centers from patients suffering from 2 retinal disease types. Experimental results show that our algorithms outperform the current state-of-the-art algorithms by a clear margin for segmentation obtaining a mean Dice Score (DS) of 82.3% for the 3 retinal fluids scoring 84.0%, 80.0%, 83.0% for Intraretinal Fluid (IRF), Subretinal Fluid (SRF), and Pigment Epithelium Detachments (PED) respectively on the testing dataset. Also we obtained a perfect Area Under the Curve (AUC) score of 100% for the detection of the presence of fluid for all 3 fluid classes on the testing dataset.

Keywords: Medical imaging, retinal fluid segmentation, Deep learning, Convolutional neural network, CNN, Optical Coherence Tomography, OCT, nnUNet, residual connection, Atrous Spatial Pyramid Pooling, ASPP.

1 Introduction

Macular Edema is an eye condition that occurs when there is a leakage of blood vessels into part of the retina called Macula (central of the eye at the back where

the vision is sharpest) and hence impairing the vision severely. There are many eye diseases that can cause this including, Age-related Macular Degeneration (AMD) and Diabetic Macular Edema (DME). Recent study [11] indicates that there's a rise of retinal diseases in Europe with more than 34 and 4 million people affected with AMD and DME respectively in the continent. AMD, is mostly common among older people (50-years and above). The early stage of AMD is asymptomatic and slows to progress to the late stage which is more severe and less common. DME, is the thickening of the retinal caused by the accumulation of intraretinal fluid in the macular and it's mostly common among diabetic patients. Currently there is no cure for these diseases and anti-vascular endothelial growth factor (Anti-VEGF) therapy is the main treatment. This requires constant administering of injections which are expensive and hence a socio-economic burden to most patients and the healthcare system. Therefore early diagnostic and active monitoring the progress of these diseases is vital because the doctors can give some behavioral advice like change of diet or doing regular exercise which will help slow down the progress or in some cases prevents the diseases from getting into a later stage. As of today this is mostly done manually which is laborious, time intensive and prone to error. Therefore an automatic and reliable tool is very crucial in this process and to further exploit the qualitative features of the retinal OCT modality efficiently. Also, the presence of eye motion artifacts in OCT lowers the signal-to-noise ratio (SNR) due to speckle noise. To circumvent this problem device manufacturers have to find a balance between achieving high SNR, image resolution and the scanning time. Hence the quality of the images varies among device vendors and hence the need to develop an automate tool with high performance that can generalise across images from all the device vendors.

To address the above issues, in this work we propose the nnUNet [8] and an enhanced version call nnUnet_RASPP. Our main contribution is enhancing the nnUNet by integrating residual blocks and an Atrous Spatial Pyramid Pooling (ASPP) block to the network's architecture.

The rest of the paper is organized as follows. A brief review of the previous studies is provided in Section 2. Section 3 presents the proposed methods. The experiment with results and visualisation are presented in Section 4, and finally, the conclusion with our contributions is described in Sections 5.

2 Background

OCT was first developed in the early 1990s but only became commercially available in 2006 and rapidly became popular due to its high image quality resolution. The segmentation of retinal OCT images have been around for many years from graph-cut [21, 23], Markov Random Fields [22, 25], level set [3, 4], to the recent Deep Learning methods that will be briefly reviewed as below.

Unet, a Deep Learning approach for medical image segmentation is introduced in [18] by Olaf Ronneberger et al. Like the name: Unet suggest, the architecture has a U-shape and consists of an encoder, bottleneck and a decoder

block. It's an end to end framework in which the encoder is use to extract features from the input images/maps, and the decoder is used for pixels localisation. At the end of the decoder path is a classification layer to classify each of the pixels to belong to each of the segmented class. Also, between the encoder and the decoder paths is a bottleneck to ensure the smooth transition from the encoder to the decoder. The encoder, decoder and bottleneck are made up of a series of convolutional layers arranged in a special order.

The Deep-ResUNet++ is presented in [15] for simultaneous segmentation of layers and fluids in retinal OCT images. The approached incorporated residual connections, ASPP blocks and Squeeze and Exciting blocks into the traditional 2D Unet [18] architecture to simultaneously segment 3 retinal layers, 3 fluids and 2 background classes from 1136 B-Scans from 24 patients suffering from wet AMD. The algorithm is validated on the Annotated Retinal OCT Images (AROI) [14] which is publicly available.

A clinical application for diagnosis and referral of retinal diseases is proposed in [6] in which 14,884 OCT B-Scans collected from 7,621 patients are trained on a framework consisting of two main parts : The segmentation model (3D Unet [29]) and the classification model.

An approach to segment fluids from retinal OCT using Graph-Theory (GT) and Fully Convolutional Networks (FCN) with curvature loss is presented in [27]. The GT is used to delineate the retinal layers, the FCN for segmentation and the loss function further uses curvature regularization term to smooth boundary and eliminate unnecessary holes inside the predicted fluid. The algorithm was validated on the RETOUCH dataset [1] consisting of 3 fluid types.

A combination of Convolutional Neural Networks (CNN) and Graph Search (GS) method is presented in [5]. The framework aims to validate nine layers boundaries from 60 retinal OCT volumes (2915 B-scans, from 20 human eyes) obtained from patients suffering from dry AMD. CNN is used for the extraction of the layer boundaries features while the GS is used for the pixels classification.

In [16] another Deep Learning approach for retinal OCT segmentation combining a FCN for segmentation with Gaussian Processes for post processing is proposed. The method is validated on the University of Miami dataset [24] which consists of 50 volumes from 10 patients suffering from diabetic retinopathy. Their approach is divided into two main steps which are the pixel classification using the FCN and the post processing using Gaussian Processes.

Another CNN-based approach for the simultaneous segmentation of layers and fluid is presented in [20]. They presented a 2D Unet like architecture with a reduced depth for the segmentation of 10 classes consisting of 8 layers, 1 background and 1 fluid from 10 patients suffering from Diabetic Macular Edema (DME). The Duke DME dataset [2] is used to validate the algorithm.

A 3-part CNN-based and Random Forest (RF) framework was developed by [12] to segment and detect fluids in OCT images. The first part of the framework is used for pre-processing of the images, the second part consists of a 2D Unet architecture for the extraction of features and a RF classifier is used at the third

part to classify the pixels. The framework is validated on the MICCAI 2017 RETOUCH challenge dataset [1].

A combination of CNN and graph-shortest path (GSP) method is presented in [17] for the segmentation and detection of fluid in retinal OCT images. The algorithm is validated on the MICCAI 2017 RETOUCH challenge dataset [1]. In this method the CNN is used for the segmentation of region of interest (ROI) and the GSP is further used for the segmentation of the layers and fluid from the ROI.

A standard double-Unet architecture for the detection and segmentation of fluids in retinal OCT images is proposed in [9]. The method uses 2 Unet architectures connected in series and is validated on the MICCAI 2017 RETOUCH challenge dataset. The output of the first Unet serves as an input to the second Unet.

nnUNet, a self-configuring framework is introduced in [8]. The framework aims to eliminate the problem of manual parameters setting "trying an error" by using the dataset's demographic features to determine and automatically set some of the model's key parameters like the batch size. The framework uses the standard Unet [18] and is evaluated on 11 biomedical image segmentation challenges consisting of 23 datasets for 53 segmentation tasks.

An extended version of the nnUNet [8] is presented by McConnell et al in [13] by integrating residual, dense, and inception blocks into the network for the segmentation of medical imaging on multiple datasets. The algorithm is evaluated on eight datasets consisting of 20 target anatomical structures.

ScSE nnU-Net, another extended version of the nnUNet [8] is presented in [26] for the segmentation of head and neck cancer tumors. It extends the original nnUNet by incorporating spatial channels with squeeze and excitation blocks into the network's architecture. The algorithm uses nnUNet to extract features from the input images/maps and then the squeeze and excitation blocks to further suppress the weaker pixels. The method was validated on the HECKTOR 2020 training dataset consisting of 201 cases and a test set of 53 cases.

In the medical image segmentation community the Unet is the most common and widely used architecture but most of the parameters are setup manually "try an error". Therefore we aim to improve the performance of the Unet by leveraging on nnUNet, a self-parameterise pipeline for medical image segmentation and adapt it to solve the problem of data source variance as explain in the next part of this paper.

3 Methods

nnUnet_RASPP is inspired and adapted from nnUNet [8] developed by Isensee et al. It is a self-configuring and automatic pipeline for medical image segmentation which helps to mitigate the problem of manual parameters setting "try an error". We enhanced the nnUNet by incorporating residual and ASPP blocks into the network's architecture. In this section we will give a brief summary of the standard Unet 3.1, nnUNet 3.2, residual connections 3.3, ASSP 3.4 block

and finally explain how we integrate these components to build nnUNet_RASPP 3.5.

3.1 Unet

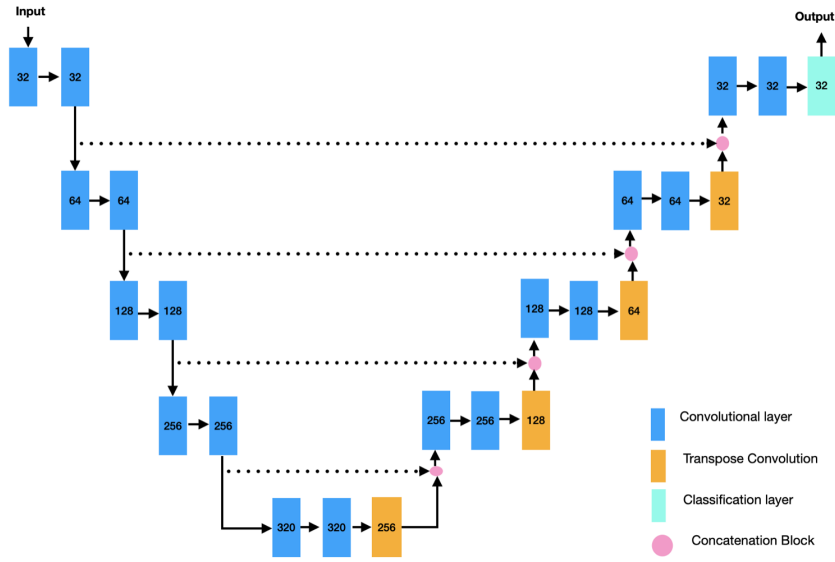


Fig. 1: An illustration of the standard Unet architecture use in nnUNet

The Unet [19] is an end to end architecture for medical image segmentation. It consists of 3 main parts : the encoder, the decoder and bottleneck between the encoder and decoder. The encoder captures contextual information (or features extraction) and reduces the size of the feature map by half after every convolutional block as we move down the encoding path by implying strided convolutions. Pixels localisation is done at the decoder. As we move up the decoder path the size of the feature map is doubled after every convolutional block by implying transposed convolutions, and for the reconstruction process features maps are concatenated to the corresponding map in the encoder path using up-sampling operations. The bottleneck serves as a bridge, linking the encoding and decoding paths together. It consists of a convolutional block that ensures a smooth transition from the encoder path to the decoder path. At the encoding path, decoding path and bridge layer each convolutional block consists of a convolutional layer that converts the pixels of the receptive field into a single value before passing it to the next operation followed by an instance normalisation to prevent over-fitting during training, and finally a LeakyReLU activation function to diminish vanishing gradient. A high level diagram to illustrate the architectural structure of the standard Unet is shown in fig 1 above.

3.2 nnUNet Overview

The nnUNet [8] is a self-configuring and automatic pipeline for medical image segmentation with the ability to automatically determine and choose the best model hyper-parameters given the data and the hardware availability, thus alleviating the problem of try an error of manual parameters setting. Given a training data the framework extracts the "data-fingerprint" such as modality, shape, and spacing and base on the hardware (GPU memory) constraints the network topology, image re-sampling methods, and input-image patch sizes are determined. After training is complete the framework determines if post-processing is needed. During training some parameters are fixed which are : learning rate that is set to 0.01, a maximum training epoch of 1000, the loss function is Cross Entropy plus Dice loss with ADAM as an optimizer, and also data augmentation is done on the fly during training. The framework uses the standard Unet [19] as the network's architecture. Please refer to the original publication [8] for more information.

3.3 Residual Connections

Residual connection is a technique use to combat the problem of vanishing gradient developed in [7]. The Unet architecture uses the chain rule for back propagation during training. This process can sometimes lead to vanishing gradient and one of the ways to circumvent this, is to introduce residual connection into the network's architecture. The diagram of residual connection is demonstrated on fig 2 below.

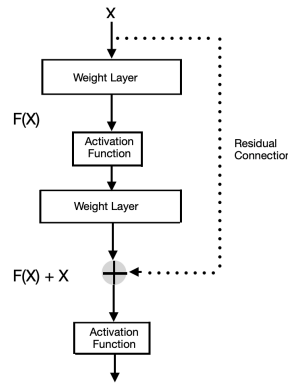


Fig. 2: An illustration of the residual connection block to combat the vanishing gradient problem where X is an input and $F(X)$ is a function of X .

3.4 Atrous Spatial Pyramid Pooling, ASPP

ASPP is a technique use to extract or capture global contextual features by applying paralleling filters with different frequencies or dilating rate for a given input filter. The diagram of residual connection is demonstrated on fig 3 below.

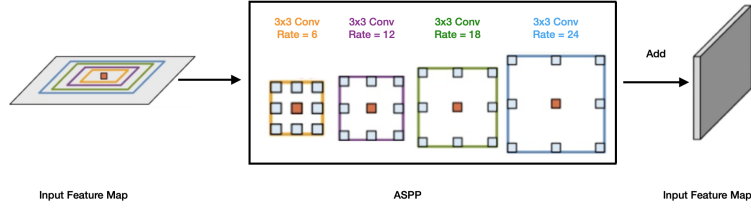


Fig. 3: An illustration of multiple parallel filters at different dilating rates or frequencies to capture global information in an ASPP block.

3.5 mnUNet_RASPP

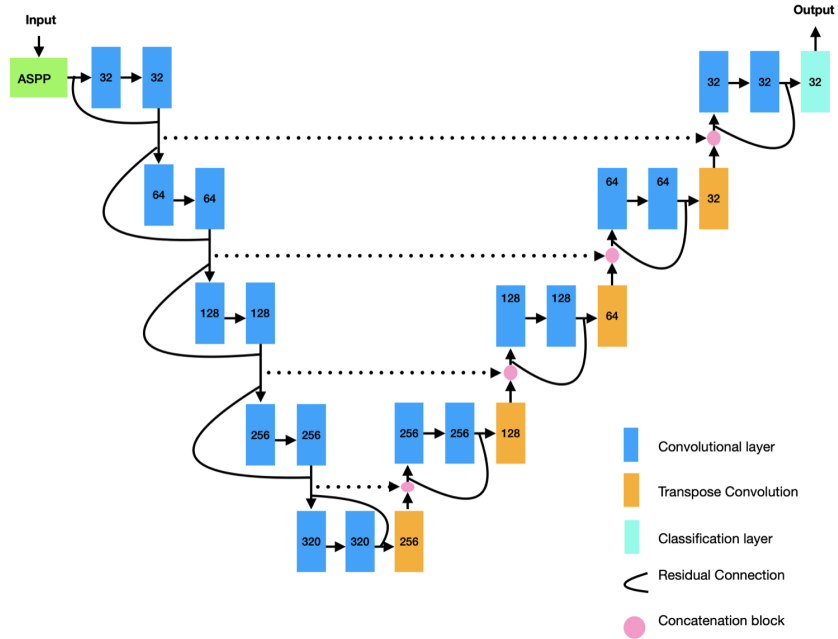


Fig. 4: A high level illustration of mnUNet_RASPP architecture with the ASPP block and the residual connections.

Inspired by the success of nnUNet [8] we have enhanced the framework by incorporating residual connections and ASPP block in the network’s architecture to solve the problem of data source variation. Residual connections were incorporated in every convolutional layer at both the encoding and decoding paths to combat the problem of vanishing gradient and the ASPP was incorporated at the input layer of the encoding path to mitigate the problem of fluid variance. The diagram of nnUnet_RASPP is demonstrated in fig 4 above.

4 Experiments

4.1 Dataset

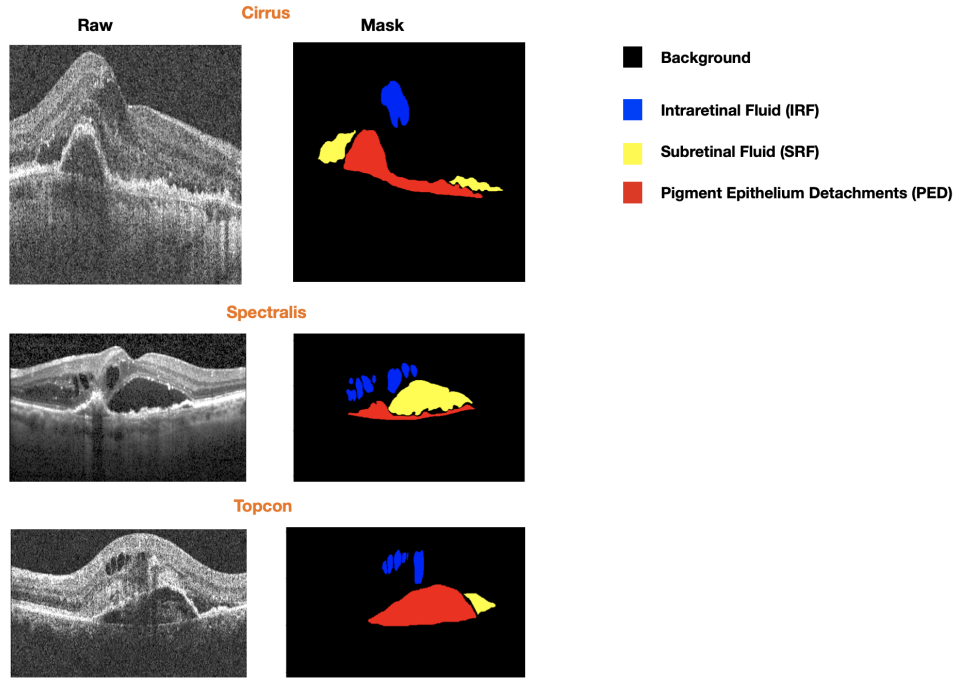


Fig. 5: B-Scan examples of raw (column 1) and their corresponded annotated mask (column 2) of OCT volumes taken from the 3 device vendors (rows): Cirrus, Spectralis and Topcon. The classes are coloured as follows : Black for the background, blue for the Intraretinal Fluid (IRF), yellow for the Subretinal Fluid (SRF) and red for the Pigment Epithelium Detachments (PED).

nnUnet_RASPP was validated on the MICCAI 2017 RETOUCH challenge dataset [1]. The dataset is publicly available and it consists of 112 OCT volumes

of patients suffering with AMD and DME collected from 3 device manufacturers: Cirrus, Spectralis and Topcon from 3 clinical centers : Medical University of Vienna (MUV) in Austria, Erasmus University Medical Center (ERASMUS) and Radboud University Medical Center (RUNMC) in The Netherlands.

The dimensions of the OCT volumes per vendor machine are as follows : Each volume of the Cirrus consists 128 B-Scans of 512×1024 pixels, Spectralis consists of 49 B-scans of 512×496 pixels and 128 B-Scans of 512×885 (T-2000) or 512×650 (T-1000) pixels for Topcon.

The training set consists of 70 volumes of 24, 24, and 22 acquired with Cirrus, Spectralis, and Topcon, respectively. Both the raw and annotated mask of the training set are made available to the public. The testing set consists of 42 OCT volumes of 14 volumes per device vendor. The raw or input of the testing set is available publicly but their corresponding annotated masks are held by the organizers of the challenge. Submission and evaluation of prediction on the testing dataset is arranged privately with the organizers and the results are sent to the participants.

Manual annotation was done by 6 grader experts from 2 medical centers : MUV (4 graders supervised by an ophthalmology resident), and RUNMC (2 graders supervised by a retinal specialist). The dataset is annotated for 4 classes of 1 background labelled as 0 and 3 fluids which are : Intraretinal Fluid (IRF) labelled as 1, Subretinal Fluid (SRF) labeled as 2 and Pigment Epithelium Detachments (PED) labelled as 3.

The RETOUCH dataset is particularly interesting because of its high level of variability. It was collected using multiple device vendors, the sizes and number of B-Scans varies per device vendor, and it was collected and annotated in multiple clinical centers. Also, for fair comparison the annotated testing set is held by the organizers and submission is curbed to a maximum of 3 per participating team.

4.2 Training and Testing

Training was done on the 70 OCT volumes of the training set (both raw and mask volumes). The estimated probabilities and predicted segmentation of the testing set (42 raw volumes) were submitted to the challenge organizers for evaluation on the ground truth or masks. Training was done for both nnUnet (as a baseline) and nnUnet_RASPP architectures. The environmental set up was the same for both architectures.

Also, to further demonstrate the robustness and generalisability of nnUnet_RASPP, the predicted segmentation of the algorithm was evaluated on OCT volumes from two vendor devices and tested on the third. In this case OCT volumes from the third vendor device weren't seen during training. For this experiment, two sets of weights were generated which are: (1) Training on 46 OCT volumes from both Spectralis (24 OCT volumes) and Topcon (22 OCT volumes) and evaluated on 14 OCT volumes from the Cirrus testing set and (2) training on 48 OCT volumes from both Cirrus (24 OCT volumes) and Spectralis (24 OCT volumes) and evaluated on 14 OCT volumes from the Topcon testing set. Again the same environmental settings were used to conduct all the experiments.

In the detection task the estimated probabilities of presence of each fluid type is plotted using the receiver operating characteristics (ROC) curve and the area under the curve (AUC) which measures the ability of a binary classifier to distinguish between classes is used as the evaluation matrix. The AUC gives a score between 0 and 1 with 1 being the perfect score and 0 is the worst. For the segmentation task, two evaluation matrices are used to measure the performance of the algorithms which are : (1) the Dice Score (DS) which is twice the intersection, divided by the union. It measures the overlapping of the pixels in the range from 0 to 1 with 1 being the perfect score and 0 being the worst. (2) The Absolute Volume Difference (AVD) which is the absolute difference between the the predicted and the ground truth. The value ranges from 0 to 1 with 0 being the best result and 1 being the worst. The equation to calculate the DS is shown on Eqn (1) and that for AVD in Eqn (2) below.

$$DSC = \frac{2|X \cap Y|}{|X| + |Y|} \quad (1)$$

$$AVD = |X| - |Y| \quad (2)$$

The models were trained on a GPU Server with NVIDIA RTX A6000 48GB.

4.3 Results

In this section we report the performance for the detection task measured by the Area Under the Curve (AUC), and the segmentation task measured by the Dice Score (DS) and Absolute Volume Difference (AVD) for the propose: nnUnet and nnUnet_RASPP, and compare our results to the current state-of-the-arts architectures.

The segmentation performance grouped by segment classes per algorithm measured in DS is illustrated in Table 1 with the corresponding diagram in Fig. 6, and that measured in AVD is illustrated in Table 2 with corresponding diagram in Fig. 7.

A detail break down of the DS and AVD per vendor device is shown in Table 3 with the corresponding diagrams of the DS and AVD in Fig. 8 and Fig. 9 respectively.

Table 4 with its corresponding diagrams in Fig. 11 show the results when trained on 2 vendor devices from the training set and tested on the third device from the holding testing set measured in DS. In this case because of the constraint of the evaluation submission (curb to 3 maximum per team) of the predicted segmentation on the testing set, results for nnUnet are unavailable.

The detection performance grouped by segment classes per algorithm measured by the AUC is illustrated in Table 5 with the corresponding diagram in Fig. 12.

The visualizations using orange arrows to highlight the fine details capture by nnUnet_RASPP when trained on two vendor devices from the training set and tested on the third from the training set are illustrated in Fig. 13 and Fig. 14. From these results, we notice the following:

1. Our propose algorithms: nnUNet_RASPP and nnUnet outperform the current state-of-the-arts architectures by a clear margin with a mean DS of 0.823 and 0.817 respectively and a mean AVD of 0.036 for nnUnet and 0.041 for nnUNet_RASPP.
2. Our propose algorithms: nnUnet obtained a perfect AUC score of 1 for all three fluid classes and nnUNet_RASPP obtained an AUC score of 0.93, 0.97, and 1.0 for the IRF, SRF, and PED respectively.
3. Also a detail break down of the DS AND AVD shows both nnUNet_RASPP and nnUnet clearly outperform the current-state-of-the-arts architectures by a clear margin for all 3 data sources.
4. We noticed an increase in performance when trained on the training set from two vendor devices and testing on the third vendor testing set scoring a mean DS of 0.84.
5. Both nnUNet_RASPP and nnUnet demonstrate a high level of robustness and generalisability with a constant high level of performance measure in DS and AVD and also when tested on dataset from a third device vendor that is not seen at training.
6. nnUNet_RASPP and nnUnet were the only two algorithms to maintain constant high level performance and generalisability across all 3 data sources.
7. Dataset acquire from Topcon was the most difficult to segment with nnUNet_RASPP and nnUnet scoring a mean DS of 0.81 each.
8. Apart from the IRF class, the nnUNet_RASPP has the best DS in every single class when compare to the other models/teams.
9. Further evaluations of the generalisability and high performance of the propose methods for training on dataset from 2 data sources and tested on the testing set of the third source that isn't seen at training show the nnUNet_RASPP architecture still outperforms the current state-of-the-arts architectures by a clear margin scoring a mean DS of 0.86 and 0.81 for Cirrus (train on Topcon and Spectralis) and Topcon (train on Cirrus and Spectralis) respectively. In this case, because of the curb of the number of submissions of the predicted segmentation for evaluation to 3 per team we are unable to show the performance of the nnUnet.

Teams	IRF	SRF	PED	Mean
nnUnet_RASPP	0.84	0.80	0.83	0.823
nnUnet	0.85	0.78	0.82	0.817
SFU	0.81	0.75	0.74	0.78
IAUNet_SPP_CL [28]	0.79	0.74	0.77	0.77
UMN	0.69	0.70	0.77	0.72
MABIC	0.77	0.66	0.71	0.71
RMIT	0.72	0.70	0.69	0.70
RetinAI	0.73	0.67	0.71	0.70
Helios	0.62	0.67	0.66	0.65
NJUST	0.56	0.53	0.64	0.58
UCF	0.49	0.54	0.63	0.55

Table 1: Table of the Dice Scores (DS) by segment classes (columns) and teams (rows) for training on the entire 70 OCT volumes of the training set and tested on the holding 42 OCT volumes from the testing set.

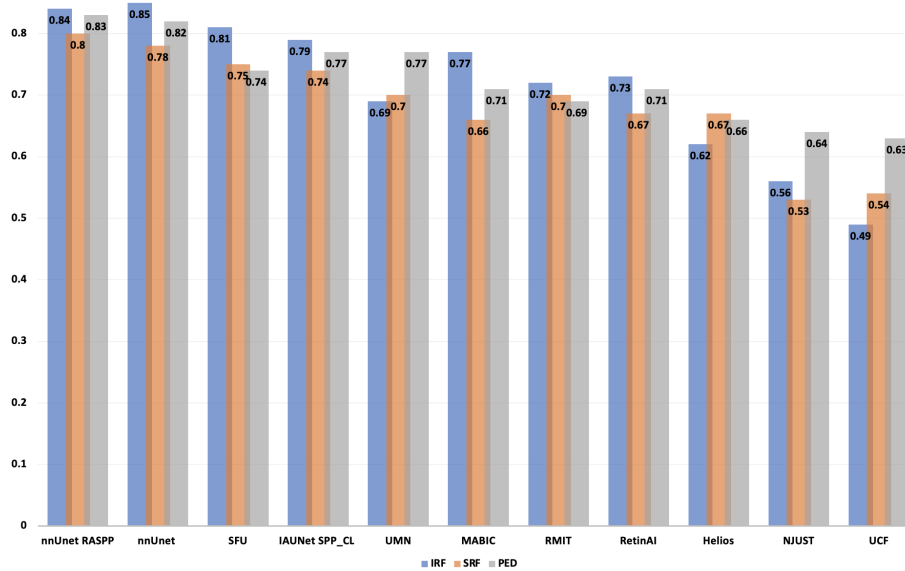


Fig. 6: Performance comparison of segmentation measure in DS of the proposed methods: nnUnet_RASPP and nnUnet, together with the current-state-of-the-arts algorithms grouped by the segment classes when trained on the entire 70 OCT volumes of the training set and tested on the holding 42 OCT volumes from the testing set.

Teams	IRF	SRF	PED	Mean
nnUNet	0.019	0.017	0.074	0.036
IAUNet_SPP_CL [28]	0.021	0.026	0.061	0.036
nnUNet_RASPP	0.023	0.016	0.083	0.041
SFU	0.030	0.038	0.139	0.069
UMN	0.091	0.029	0.114	0.078
MABIC	0.027	0.059	0.163	0.083
RMIT	0.040	0.072	0.1820	0.098
RetinAI	0.077	0.0419	0.2374	0.118
Helios	0.0517	0.055	0.288	0.132
NJUST	0.1130	0.0963	0.248	0.153
UCF	0.2723	0.1076	0.2762	0.219

Table 2: Table of the Absolute Volume Difference (AVD) by segment classes (columns) and teams (rows) for training on the entire 70 OCT volumes of the training set and tested on the holding 42 OCT volumes from the testing set.

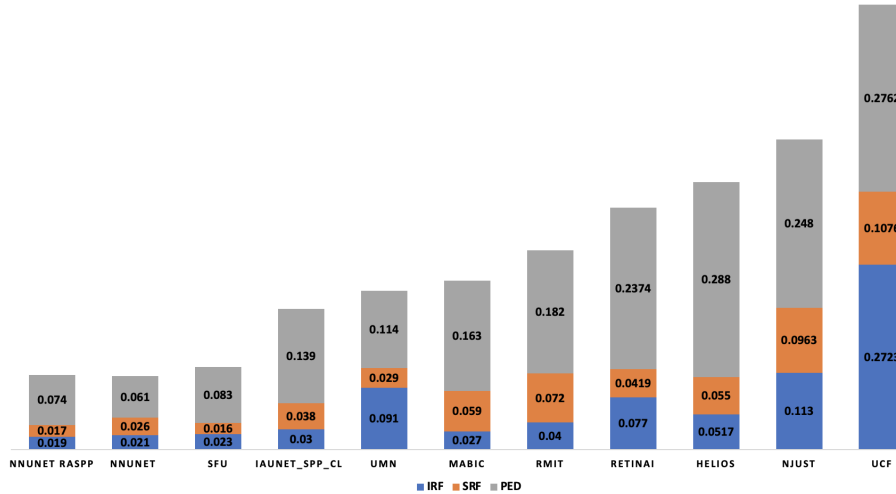


Fig. 7: Performance comparison of segmentation measure in AVD of the proposed methods: nnUNet_RASPP and nnUNet, together with the current-state-of-the-arts algorithms grouped by the segment classes when trained on the entire 70 OCT volumes of the training set and tested on the holding 42 OCT volumes from the testing set.

Cirrus						
Teams	IRF		SRF		PED	
nnUnet_RASPP	0.91	0.00670	0.80	0.00190	0.89	0.021700
nnUnet	0.91	0.00850	0.80	0.00190	0.88	0.02060
SFU	0.83	0.020388	0.72	0.008069	0.73	0.116385
UMN	0.73	0.076024	0.62	0.007309	0.82	0.023110
MABIC	0.79	0.018695	0.67	0.008188	0.73	0.091524
RMIT	0.85	0.037172	0.64	0.005207	0.76	0.079259
RetinAI	0.77	0.046548	0.66	0.008857	0.82	0.040525
Helios	0.70	0.038073	0.66	0.008313	0.69	0.097135
NJUST	0.57	0.077267	0.55	0.024092	0.69	0.144518
UCF	0.57	0.174140	0.54	0.028924	0.66	0.215379
Spectralis						
Teams	IRF		SRF		PED	
nnUnet_RASPP	0.89	0.030100	0.68	0.008400	0.81	0.068600
nnUnet	0.89	0.031400	0.62	0.012600	0.80	0.073600
SFU	0.87	0.033594	0.73	0.020017	0.76	0.135562
UMN	0.76	0.072541	0.72	0.013499	0.74	0.121404
MABIC	0.83	0.036273	0.59	0.033384	0.75	0.181842
RMIT	0.69	0.121642	0.67	0.026377	0.70	0.228323
RetinAI	0.77	0.026921	0.65	0.036062	0.71	0.120528
Helios	0.61	0.030149	0.53	0.035625	0.63	0.330431
NJUST	0.60	0.080740	0.38	0.076071	0.52	0.412231
UCF	0.41	0.407741	0.31	0.155769	0.52	0.414739
Topcon						
Teams	IRF		SRF		PED	
nnUnet_RASPP	0.72	0.032500	0.93	0.037800	0.78	0.157300
nnUnet	0.74	0.015900	0.92	0.036300	0.78	0.127700
SFU	0.72	0.039515	0.80	0.085907	0.74	0.164926
UMN	0.59	0.125454	0.77	0.066680	0.76	0.197794
MABIC	0.68	0.025097	0.73	0.134050	0.65	0.215687
RMIT	0.63	0.072609	0.78	0.094004	0.60	0.404842
RetinAI	0.66	0.045674	0.70	0.171808	0.60	0.385178
Helios	0.56	0.086773	0.81	0.119888	0.65	0.435057
NJUST	0.52	0.181237	0.66	0.188827	0.70	0.187733
UCF	0.48	0.235298	0.76	0.134283	0.61	0.200602

Table 3: Table of the Dice Score (DS) and Absolute Volume Difference (AVD) by segment classes (columns) and teams (rows) for training on the entire 70 OCT volumes of the training set and tested on the holding 42 OCT volumes from the testing set per device.

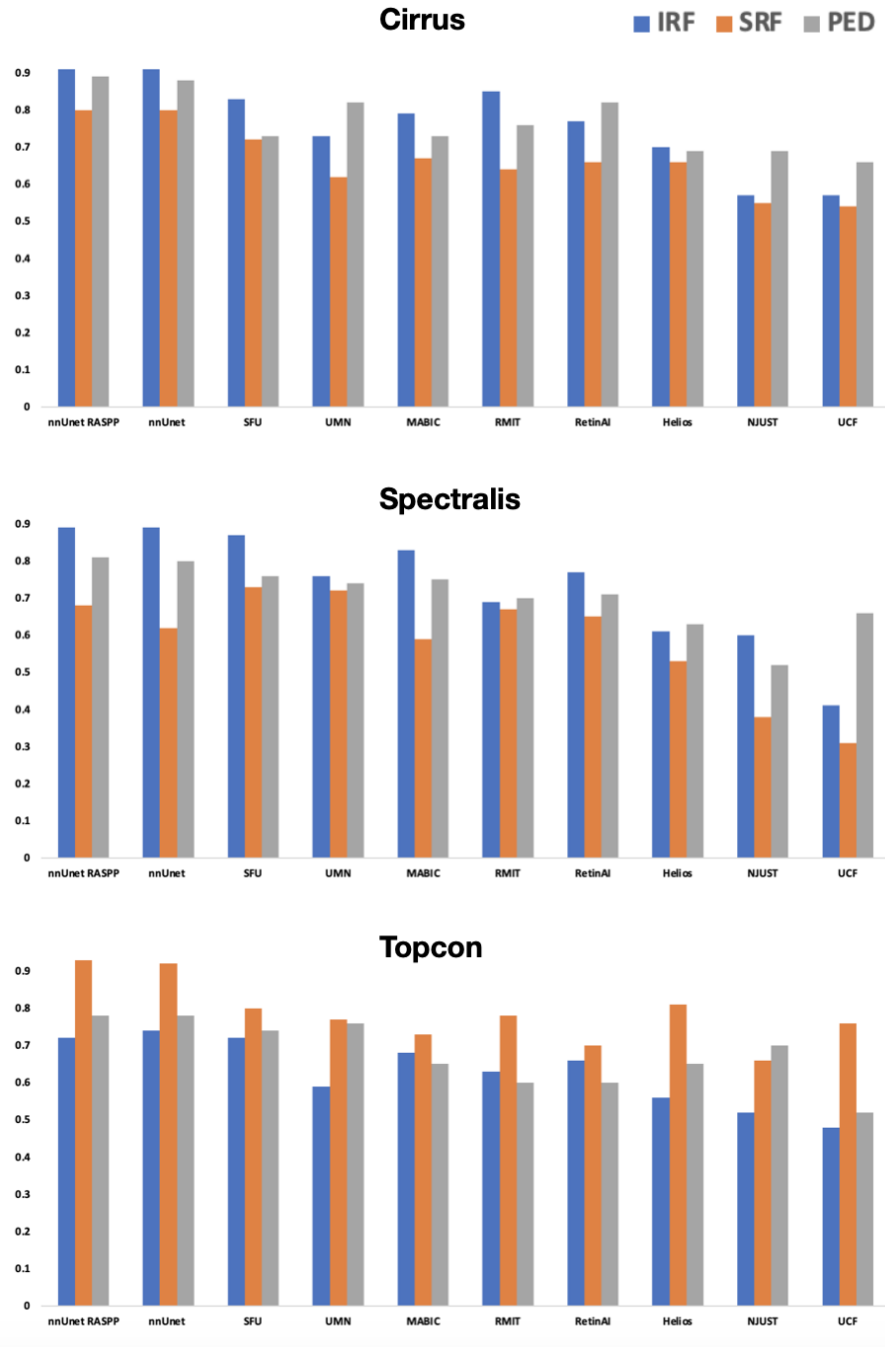


Fig. 8: Performance comparison of segmentation measure in DS of the proposed methods: nnUnet_RASPP and nnUnet, together with the current-state-of-the-arts algorithms grouped by the segment classes when trained on the entire 70 OCT volumes of the training set and tested on the holding 42 OCT volumes from the testing set per device.

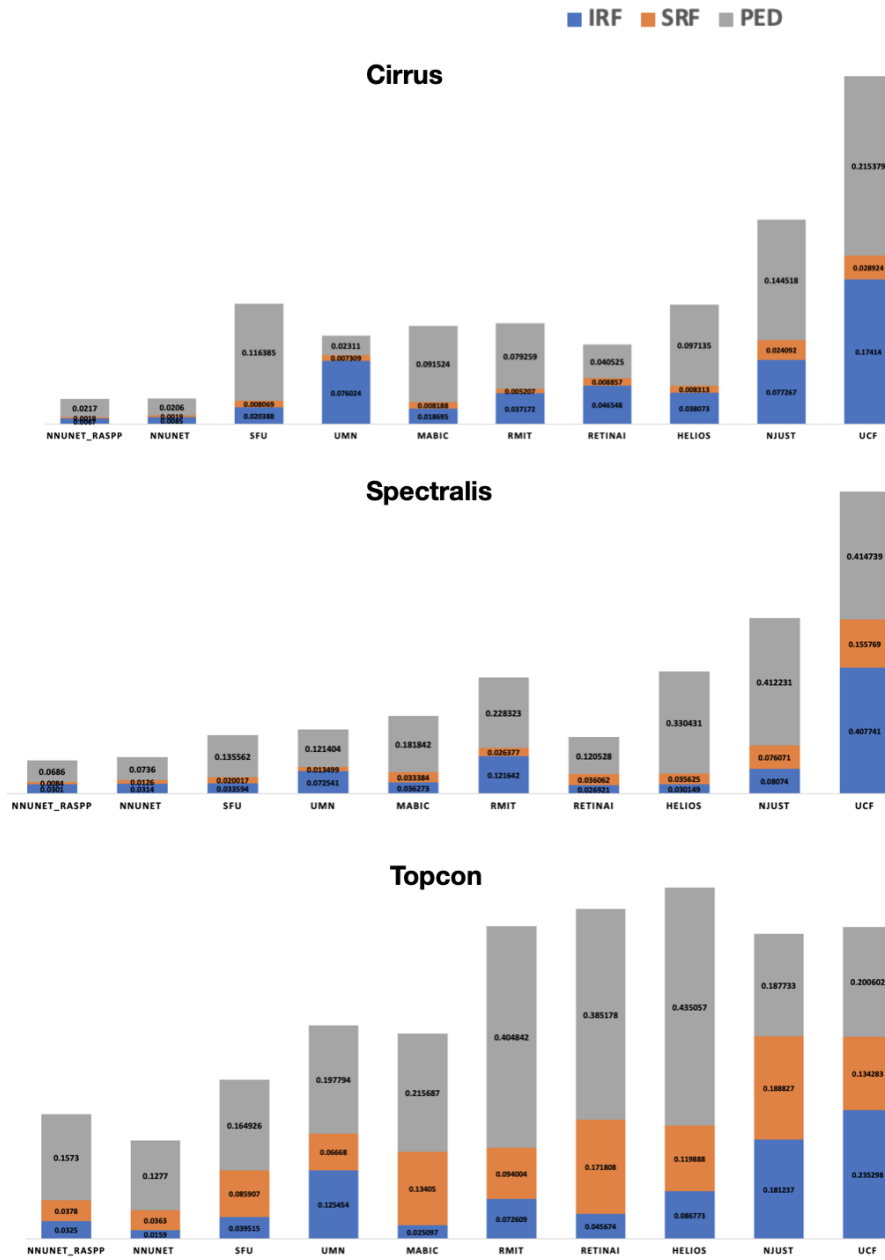


Fig. 9: Performance comparison of segmentation measure in AVD of the proposed methods: nnUnet_RASPP and nnUnet, together with the current-state-of-the-arts algorithms grouped by the segment classes when trained on the entire 70 OCT volumes of the training set and tested on the holding 42 OCT volumes from the testing set per device.

Cirrus								
Teams	IRF		SRF		PED		Mean	
nnUnet_RASPP	0.90	0.0122	0.78	0.0031	0.89	0.019	0.86	0.0114
SFU	0.83	0.0204	0.72	0.0081	0.73	0.1164	0.76	0.0483
UMN	0.73	0.0760	0.62	0.0073	0.82	0.0231	0.72	0.0355
MABIC	0.79	0.0187	0.67	0.0082	0.73	0.0915	0.73	0.0395
RMIT	0.85	0.0372	0.64	0.0052	0.76	0.0793	0.75	0.0406
RetinAI	0.77	0.0466	0.66	0.0089	0.82	0.0405	0.75	0.0320
Helios	0.70	0.0381	0.66	0.0083	0.69	0.0971	0.68	0.0478
SVDNA [10]	0.61	–	0.66	–	0.74	–	0.67	–
NJUST	0.57	0.0773	0.55	0.0241	0.69	0.1446	0.60	0.0820
UCF	0.57	0.1741	0.54	0.0289	0.66	0.2154	0.59	0.1395
Topcon								
Teams	IRF		SRF		PED		Mean	
nnUnet_RASPP	0.72	0.0201	0.93	0.0298	0.78	0.2119	0.81	0.0873
SFU	0.72	0.0395	0.80	0.0859	0.74	0.1649	0.75	0.0968
UMN	0.59	0.1255	0.77	0.0667	0.76	0.1978	0.71	0.1300
SVDNA [10]	0.61	–	0.80	–	0.72	–	0.71	–
MABIC	0.68	0.0251	0.73	0.1341	0.65	0.2157	0.69	0.1250
RMIT	0.63	0.0726	0.78	0.0940	0.60	0.4048	0.67	0.1905
RetinAI	0.66	0.0457	0.70	0.1718	0.60	0.3852	0.65	0.2009
Helios	0.56	0.0868	0.81	0.1199	0.65	0.4351	0.67	0.2139
NJUST	0.52	0.1812	0.66	0.1888	0.70	0.1877	0.63	0.1859
UCF	0.48	0.2353	0.76	0.1343	0.61	0.2006	0.62	0.1900

Table 4: Table of the DS and AVD by segment classes (columns) and teams (rows) trained on 48 OCT volumes from 2 device sources and evaluated on 14 OCT volumes from the testing set on the third device that wasn’t seen at training.

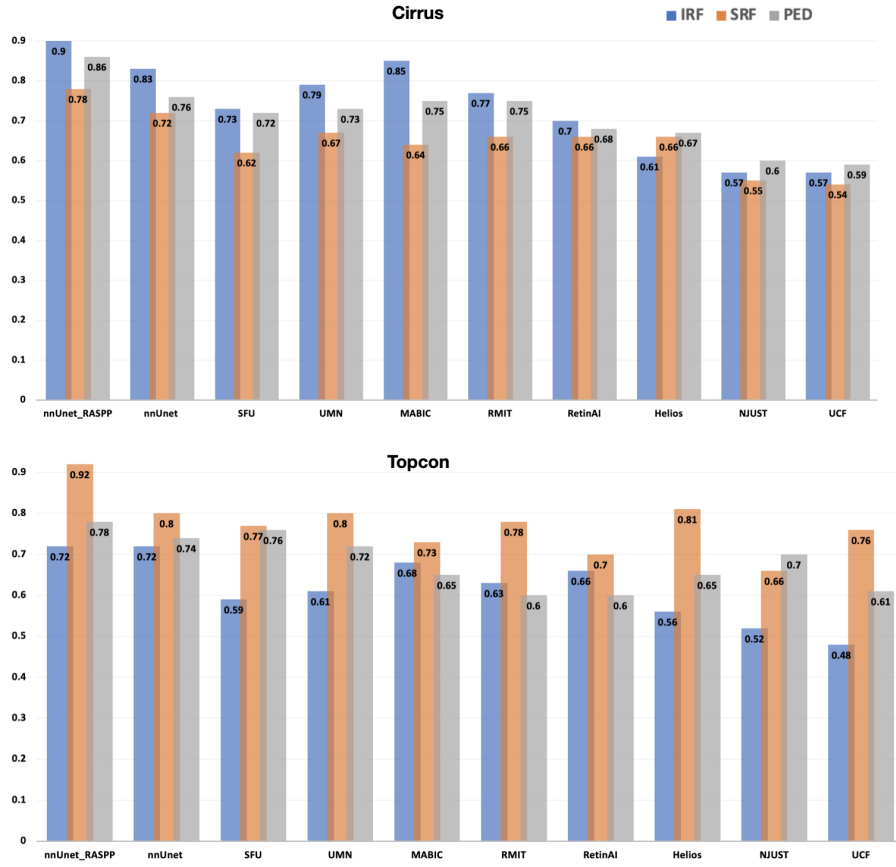


Fig. 10: Performance comparison of segmentation measure in DS of the propose nnUnet_RASPP, together with the current-state-of-the arts algorithms group by the segment classes train on 46 OCT volumes from both Spectralis (24 OCT volumes) and Topcon (22 OCT volumes) and evaluated on the holding testing set (cirrus top and Topcon below).

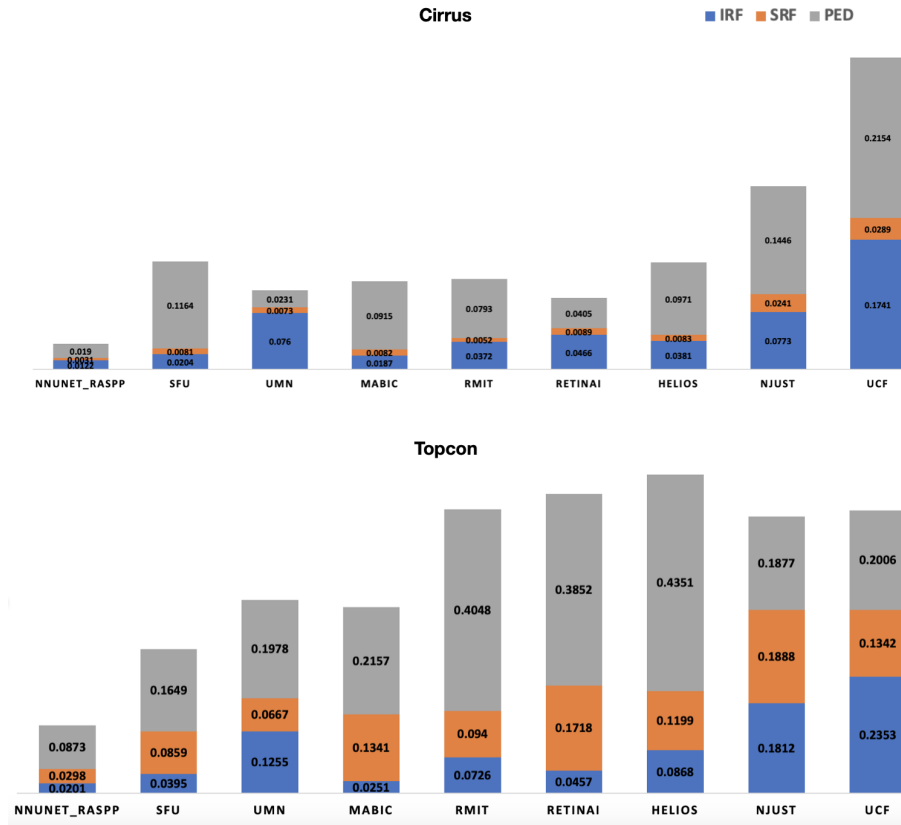


Fig. 11: Performance comparison of segmentation measure in AVD of the propose nnUNet_RASPP, together with the current-state-of-the arts algorithms group by the segment classes train on 46 OCT volumes from both Spectralis (24 OCT volumes) and Topcon (22 OCT volumes) and evaluated on the holding testing set (cirrus top and Topcon bottom).

Teams	IRF	SRF	PED	Mean
nnUnet	1.0	1.0	1.0	1.0
SFU	1.0	1.0	1.0	1.0
nnUnet_RASPP	0.93	0.97	1.0	0.97
Helios	0.93	1.0	0.97	0.97
UCF	0.94	0.92	1.0	0.95
MABIC	0.86	1.0	0.97	0.94
UMN	0.91	0.92	0.95	0.93
RMIT	0.71	0.92	1.0	0.88
RetinAI	0.99	0.78	0.82	0.86
NJUST	0.70	0.83	0.98	0.84

Table 5: Table of the Area Under the Curve (AUC) by segment classes (columns) and teams (rows) for training on the entire 70 OCT volumes of the training set and tested on the holding 42 OCT volumes from the testing set.

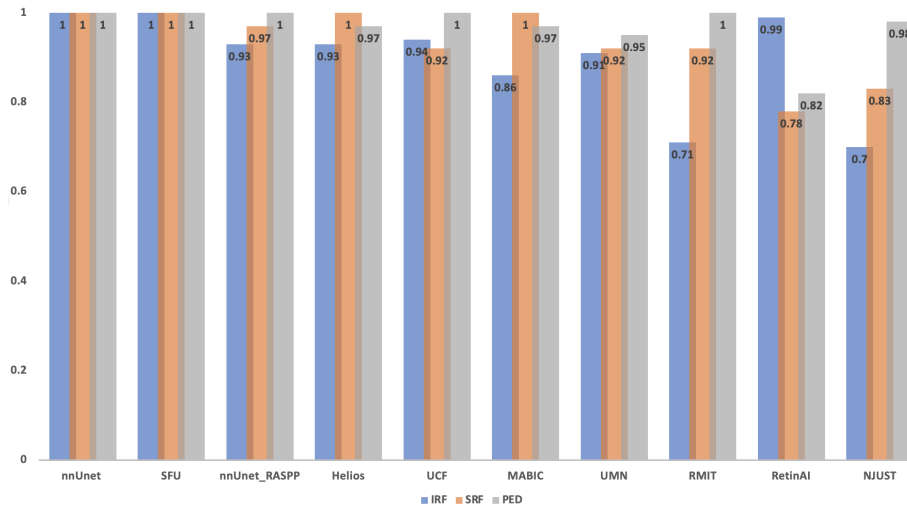


Fig. 12: Performance comparison of the detection measure in AUC of the proposed methods: nnUnet_RASPP and nnUnet, together with the current-state-of-the-arts algorithms grouped by the segment classes when trained on the entire 70 OCT volumes of the training set and tested on the holding 42 OCT volumes from the testing set.

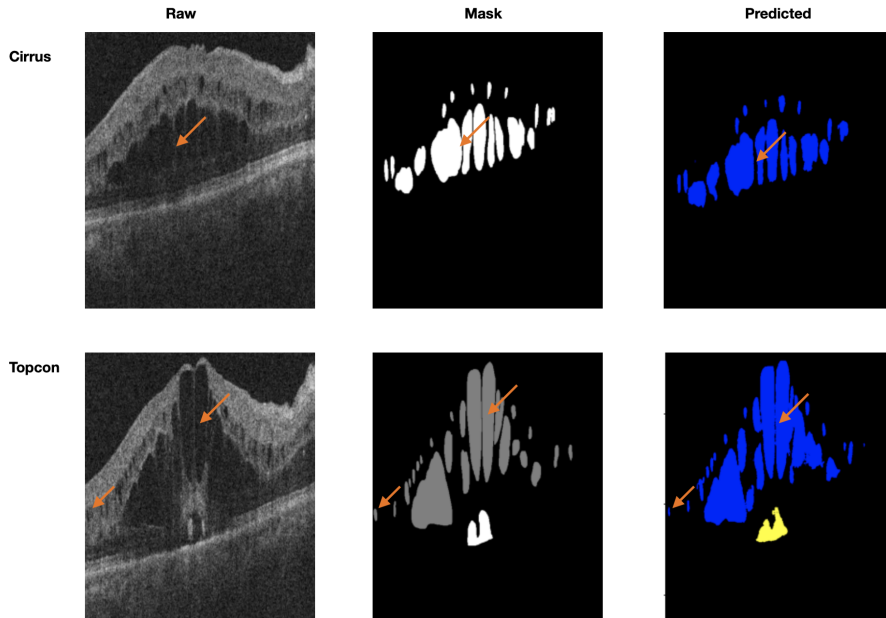


Fig. 13: Examples of B-Scans to illustrate the visualization output/predicted of nnUNet_RASPP, in order of the raw/inputs, mask/annotations and predicted/outputs in columns when trained on the training set of two vendor devices and tested on the training set of the third vendor device (Cirrus and Topcon in row 1 and row 2 respectively). Fine details capture by the model are indicated with orange arrows.

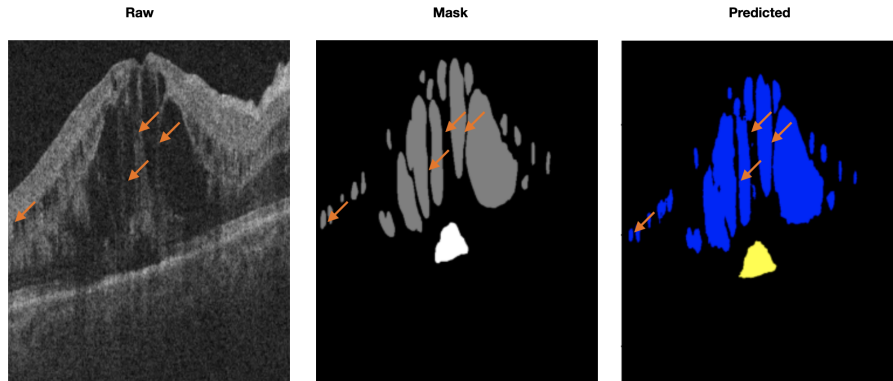


Fig. 14: An example of a B-Scan to illustrate the visualization output/predicted of nnUnet_RASPP, in order of the raw/inputs, mask/annotations and predicted/outputs when zoom out to highlights the fine details capture by the model using orange arrows. This is capture when trained on the training set of the Spectralis and Topcon devices and tested on the training set of the Cirrus device.

5 Conclusions

In this work, we have investigated the problem of detection and segmentation of multiple fluids in retinal OCT volumes acquired from multiple device vendors. Inspired by the success of the nnUNet [8] we have enhanced the model’s architecture to build a novel algorithm call nnUnet_RASPP. Both nnUNet and nnUnet_RASPP were evaluated on the MICCAI 2017 RETOUCH challenge dataset [1]. We submitted predictions for both architectures and experimental results show that for the current league table and other known published results our algorithms outperform the current state-of-the-arts architectures by a clear margin as they occupy the first and second places for the DS, AVD and AUC evaluation.

Our main contribution is : we have enhanced the nnUNet by incorporating the residual blocks and ASPP block into the network’s architecture to solve this particular problem.

The propose algorithms provide useful information for further diagnosis and monitoring the progress of retinal diseases such as AMD, DME and Glaucoma. In the future we look to investigate our algorithms on other medical image datasets once they are available publicly.

References

1. Hrvoje Bogunović, Freerk Venhuizen, Sophie Klimscha, Stefanos Apostolopoulos, Alireza Bab-Hadiashar, Ulas Bagci, Mirza Faisal Beg, Loza Bekalo, Qiang Chen, Carlos Ciller, et al. Retouch: the retinal oct fluid detection and segmentation benchmark and challenge. *IEEE transactions on medical imaging*, 38(8):1858–1874, 2019.
2. Stephanie Chiu, Michael Allingham, Priyatham Mettu, Scott Cousins, Joseph Izatt, and Sina Farsiu. Kernel regression based segmentation of optical coherence tomography images with diabetic macular edema. *Biomedical Optics Express*, 6, 04 2015.
3. Bashir Isa Dodo, Yongmin Li, Djibril Kaba, and Xiaohui Liu. Retinal layer segmentation in optical coherence tomography images. *IEEE Access*, 7:152388–152398, 2019.
4. Bashir Isa Dodo, Yongmin Li, and Xiaohui Liu. Level set segmentation of retinal oct images. In *International Conference on Bioimaging. Czech Republic.*, 2019.
5. Leyuan Fang, David Cunefare, Chong Wang, Robyn H Guymer, Shutao Li, and Sina Farsiu. Automatic segmentation of nine retinal layer boundaries in oct images of non-exudative amd patients using deep learning and graph search. *Biomedical optics express*, 8(5):2732–2744, 2017.
6. Jeffrey Fauw, Joseph Ledsam, Bernardino Romera-Paredes, Stanislav Nikolov, Nenad Tomasev, Sam Blackwell, Harry Askham, Xavier Glorot, Brendan O’Donoghue, Daniel Visentin, George Driessche, Balaji Lakshminarayanan, Clemens Meyer, Faith Mackinder, Simon Bouton, Kareem Ayoub, Reena Chopra, Dominic King, Alan Karthikesalingam, and Olaf Ronneberger. Clinically applicable deep learning for diagnosis and referral in retinal disease. *Nature Medicine*, 24, 09 2018.
7. Kaiming He, Xiangyu Zhang, Shaoqing Ren, and Jian Sun. Deep residual learning for image recognition. In *Proceedings of the IEEE conference on computer vision and pattern recognition*, pages 770–778, 2016.
8. Fabian Isensee, Paul F Jaeger, Simon AA Kohl, Jens Petersen, and Klaus H Maier-Hein. nnu-net: a self-configuring method for deep learning-based biomedical image segmentation. *Nature methods*, 18(2):203–211, 2021.
9. Sung Ho Kang, Hyoung Suk Park, Jaeseong Jang, and Kiwan Jeon. Deep neural networks for the detection and segmentation of the retinal fluid in oct images. *MICCAI Retinal OCT Fluid Challenge (RETOUCH)*, 2017.
10. Valentin Koch, Olle Holmberg, Hannah Spitzer, Johannes Schiefelbein, Ben Asani, Michael Hafner, and Fabian J Theis. Noise transfer for unsupervised domain adaptation of retinal oct images. In *Medical Image Computing and Computer Assisted Intervention–MICCAI 2022: 25th International Conference, Singapore, September 18–22, 2022, Proceedings, Part II*, pages 699–708. Springer, 2022.
11. Jeany Q Li, Thomas Welchowski, Mathias Schmid, Julia Letow, A Caroline Wolpers, Frank G Holz, and Robert P Finger. Retinal diseases in europe. *European Society of Retina Specialists (EURETINA)*, 2017.
12. Donghuan Lu, Morgan Heisler, Sieun Lee, Gavin Ding, Marinko V Sarunic, and Mirza Faisal Beg. Retinal fluid segmentation and detection in optical coherence tomography images using fully convolutional neural network. *arXiv preprint arXiv:1710.04778*, 2017.
13. Niccolo McConnell, Alina Miron, Zidong Wang, and Yongmin Li. Integrating residual, dense, and inception blocks into the nnunet. In *2022 IEEE 35th International*

- Symposium on Computer-Based Medical Systems (CBMS)*, pages 217–222. IEEE, 2022.
14. Martina Melinscak, Marin Radmilović, Sven Loncaric, and Zoran Vatauvuk. Annotated retinal optical coherence tomography images (aroi) database for joint retinal layer and fluid segmentation. *Automatika*, 62:375–385, 08 2021.
 15. Nchongmaje Ndipenoch, Alina Miron, Zidong Wang, and Yongmin Li. Simultaneous segmentation of layers and fluids in retinal oct images. In *2022 15th International Congress on Image and Signal Processing, BioMedical Engineering and Informatics (CISP-BMEI)*, pages 1–6. IEEE, 2022.
 16. Mike Pekala, Neil Joshi, TY Alvin Liu, Neil M Bressler, D Cabrera DeBuc, and Philippe Burlina. Deep learning based retinal oct segmentation. *Computers in biology and medicine*, 114:103445, 2019.
 17. Abdolreza Rashno, Dara D Koozekanani, and Keshab K Parhi. Detection and segmentation of various types of fluids with graph shortest path and deep learning approaches. *Proc. MICCAI Retinal OCT Fluid Challenge (RETOUCH)*, pages 54–62, 2017.
 18. Olaf Ronneberger, Philipp Fischer, and Thomas Brox. U-net: Convolutional networks for biomedical image segmentation. In *International Conference on Medical image computing and computer-assisted intervention*, pages 234–241. Springer, 2015.
 19. Olaf Ronneberger, Philipp Fischer, and Thomas Brox. U-net: Convolutional networks for biomedical image segmentation. In *Medical Image Computing and Computer-Assisted Intervention–MICCAI 2015: 18th International Conference, Munich, Germany, October 5–9, 2015, Proceedings, Part III 18*, pages 234–241. Springer, 2015.
 20. Abhijit Guha Roy, Sailesh Conjeti, Sri Phani Krishna Karri, Debdoot Sheet, Amin Katouzian, Christian Wachinger, and Nassir Navab. Relaynet: retinal layer and fluid segmentation of macular optical coherence tomography using fully convolutional networks. *Biomedical optics express*, 8(8):3627–3642, 2017.
 21. Ana Salazar-Gonzalez, Djibril Kaba, Yongmin Li, and Xiaohui Liu. Segmentation of the blood vessels and optic disk in retinal images. *IEEE journal of biomedical and health informatics*, 18(6):1874–1886, 2014.
 22. Ana Salazar-Gonzalez, Yongmin Li, and Djibril Kaba. MRF reconstruction of retinal images for the optic disc segmentation. In *International Conference on Health Information Science*, pages 88–99, 2012.
 23. Ana G Salazar-Gonzalez, Yongmin Li, and Xiaohui Liu. Retinal blood vessel segmentation via graph cut. In *International Conference on Control Automation Robotics & Vision*, pages 225–230, 2010.
 24. Jing Tian, Boglarka Varga, Erika Tatrai, Palya Fanni, Gabor Mark Somfai, William E Smiddy, and Delia Cabrera Debuc. Performance evaluation of automated segmentation software on optical coherence tomography volume data. *Journal of biophotonics*, 9(5):478–489, 2016.
 25. Chuang Wang, Y Wang, and Yongmin Li. Automatic choroidal layer segmentation using markov random field and level set method. *IEEE journal of biomedical and health informatics*, 2017.
 26. Juanying Xie and Ying Peng. The head and neck tumor segmentation using nnunet with spatial and channel ‘squeeze & excitation’ blocks. In *Head and Neck Tumor Segmentation: First Challenge, HECKTOR 2020, Held in Conjunction with MICCAI 2020, Lima, Peru, October 4, 2020, Proceedings 1*, pages 28–36. Springer, 2021.

27. Gang Xing, Li Chen, Hualin Wang, Jiong Zhang, Dongke Sun, Feng Xu, Jianqin Lei, and Xiayu Xu. Multi-scale pathological fluid segmentation in oct with a novel curvature loss in convolutional neural network. *IEEE Transactions on Medical Imaging*, 41(6):1547–1559, 2022.
28. Gang Xing, Li Chen, Hualin Wang, Jiong Zhang, Dongke Sun, Feng Xu, Jianqin Lei, and Xiayu Xu. Multi-scale pathological fluid segmentation in oct with a novel curvature loss in convolutional neural network. *IEEE Transactions on Medical Imaging*, 41(6):1547–1559, 2022.
29. Özgün Çiçek, Ahmed Abdulkadir, Soeren Lienkamp, Thomas Brox, and Olaf Ronneberger. 3d u-net: Learning dense volumetric segmentation from sparse annotation. 06 2016.